WORLD CONFERENCE ON TIMBER ENGINEERING 2025
BRISBANE, AUSTRALIA
Advancing Timber for the Future Built Environment

ESTIMATION OF TEMPERATURE PROFILE WITHIN STEEL BAR-TIMBER COMPOSITE BEAM USING DATA OF COMBUSTION TEST

Shinichi Shioya [1] and Shizuka Matsushita[2]

ABSTRACT: Recently, timber buildings are desired from a viewpoint of global warming, and moreover, in severe earthquake prone zones, such as Japan, they are more desired on the grounds of light weight of timber members. We are developing a frame system formed by hybrid timber members strengthened with deformed steel bars (i.e. rebars) using epoxy resin adhesive. To practice the system, it is necessary to investigate fire resistance performance of the members. As a trial, we conducted a 60-minute burn test of one relatively small cross section of a steel bar-timber composite beam and reported its results in previous WCTE 2023. Now, for practical use, we have conducted a 60-minute combustion test of three beams with relatively large cross sections and reports the experiments and their results in WCTE 2025. By further improving the previous proposed in WCTE2023[1], the temperature profile in beam was calculated by the method, and strength capacity and failure form of the beam tested were examined. This report describes the improved method and results of the investigation of the calculated capacity and fracture mode.

KEYWORDS: *Fire, Beam, Temperature profile, Steel bar-timber composite member, Deformed steel bar*

1 – INTRODUCTION

Nowadays, the cross laminated timber (CLT) is being used for buildings. However, CLT often restricts planning of buildings because it is flat plate member. To improve the flexibility of the planning, higher stiffness and strength are desired for column and beam. We have been developing a frame system formed with steel bar-timber composite members which can perform better than those of reinforced concrete structure [1]. To practice the system, it is necessary to investigate fire resistance performance of the members. As a trial, we conducted a 60-minute combustion test of a composite beam with one relatively small cross section and reported a new calculation method for temperature profile within the beam in previous WCTE 2023[2]. Now, for practical use, we have conducted a 60-minute burn test of three beams with relatively large cross sections and reports the experiments and results in WCTE 2025[3]. By further improving the proposed method, temperature profile in beam was calculated by the method, and strength capacity and fracture form of the beam tested were examined.

2–FUNCTION OF TEMPERATURE PROFILE DURING HEATING

2.1 STRATEGY

Establishing a method for estimating temperature profile in a cross-section indicates identifying the function $T(x,y,t)$ of temperature at any point (x,y) within the cross-section at a heating time t. The function includes constants. The function $T(x,y,t)$ is derived by fitting those values to the temperature-heating time curve (T-t curve) measured in a combustion test.

2.2 ASSUMPTION

1) It is assumed that a slab is placed on the top surface of a beam, and that the bottom and side surfaces of the beam are heated with the same temperature history. It is assumed that the top surface is not radiated from the slab.
2) In Figure 1, the symbols/d_{mL}, d_{ms1}, d_{ms2}, represent the vertical and horizontal distances from the bottom and sides of the beam to a special point/m within the cross-section of the beam. These distances are collectively referred to as d_m. The difference in the component of the temperature rise due to heating from three sides (hereafter, 3-direction heating) is assumed to depend only on the magnitude of d_m.
3) Temperature of test specimen before heating is assumed to be room temperature/T_r. Charring temperature of wood/T_c is done to be 300℃. The target temperature is done to range from T_r to T_c, and any temperature outside this range

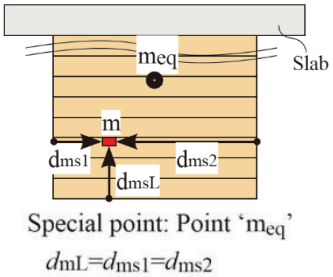

Figure 1: Distances from 3-directions and the special point 'm_{eq}'

[1] Shinichi Shioya, Department of Architecture, Kagoshima University, Kagoshima, Japan, k7347039@kadai.jp

[2] Shizuka Matsushita, Ishimoto Architectural Design Company, Tokyo, Japan, k3608908@kadai.jp

https://doi.org/10.52202/080513-0188

is done to be out of target of its estimation.

4) The temperature of the air inside a furnace immediately after heating starts and the temperature of the beam surface are low, and there is a difference between the time when heating starts and the time when the beam surface starts to char, but it is assumed that the difference can be ignored and the time when heating starts be taken as the time when the beam surface starts to char. This causes errors in the temperature estimated for the region close to the surfaces. However, in the case of semi-fireproof structures, the heating is assumed to be carried out for a certain period, so the error is not a problem at the end of the heating period.

5) The temperature function/T (x, y, t) at any point at (x, y) in the cross-section of a beam at the time/t is expressed as the sum of the temperature rise components due to heating from each surface added to the temperature/T_r. Note that our method applies to the case where the beam width is greater than a certain value depending on the heating time, when the beam is heated on three sides.

2.3 MAPPING ONTO TEMPERATURE-CHARRED BODER DISTANCE CURVE/T-S CURVE AND ITS MERIT

The temperature-time curve (T-t curve) as shown in Figure 10(a) and Figure 11(a) can be measured using thermocouples inside the beam. Measuring points can be freely selected, and we define them measuring point/m. Temperature rise rate history can be clarified from the T-t curve; if the charring temperature/T_c can be specified, the time/t_c when takes to reach charring temperature can also be specified. By dividing the wood depth dm at the m-point by the time/t_c, the average charring rate/v_c up to the temperature/T_c can also be calculated. Herein, for modelling the temperature profile, we define v_c based on the charring temperature. It is hard to find a function for estimating change in temperature rise between room temperature/T_r and charring temperature/T_c on the T-t curve. Therefore, we use the charring rate/v_c to convert the heating time/t on the horizontal axis in Figure 2 into the distance/S from the measuring point m to the charring border using Equation (1) and map the temperature-heating time curve (T-t curve) onto the temperature-charring border distance curve (T-S curve).

$$S = d_m - v_c\, t \tag{1}$$

where, d_m: the depth of wood from the surface of beam to the measurement point/m, v_c: charring rate (mm/min), t: heating time (min)

In a beam with a slab, three sides are heated, but for simplicity of the modelling, we will first discuss the case of one-sided heating (one-direction heating). Figure 2 shows a schematic diagram of the T-S curve for the measuring point/m in the case of one-direction

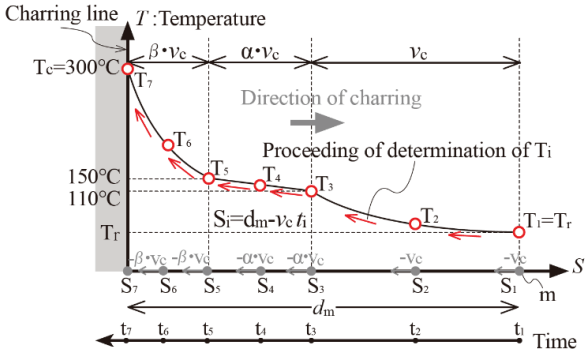

Figure 2: *T-S curve of measurement point 'm'*

heating. The red arrows mean the path from the start of heating. The path is one for the case where the depth of wood/d_m is relatively large. In the T-S curve, when the distance/S is equal to d_m at the start of heating, the temperature/T_m is room temperature/T_r, and at the distance/S being zero, T_m equals the charring temperature/T_c. These clear boundary values exist. In addition, as the heating progresses, the charring border approaches the measuring point/m, but for the charring border, it can be assumed that the measuring point/m approaches at the charring rate/v_c. For the distance/S being large, the rate of temperature rise is slow, and for its being small, it increases rapidly. The function of the T-S curve is required to satisfy the clear boundary values and the trends of the change. The distance/S is calculated using the heating time/t according to Equation (1); hence, finding the characteristics of the temperature rise in the T-S curve is equivalent to finding the characteristics of the temperature rise rate in the T-t curve. By inverting the T-S curve obtained by mapping, the T-t curve can also be approximated, and the boundary values and change trends can be reflected in the T-t curve. This is the strong merit of the mapping used in this theory. Another merit is that, as seen in Equation (1), the distance/S includes the three-depth/d_m of the measuring point/m. This means that the location of the measuring point is included in the function of the T-S curve, and effects of d_m can be reflected in the T-t curve that is inverse mapped.

2.4 FUNCTION FOR T-S CURVE UNDER ONE-DIERCTION HEATING

Equation (2) is suitable as an approximating function for the temperature/T_m of the measuring point/m at heating time/t. The reasoning behind this is explained below. Substituting Equation (1) into Equation (2), we obtain Equation (3), and the component of temperature rise (T-Tr) is expressed as Equation (4). By dividing both sides of Equation (4) by (Tc -Tr) and expressing the result as a dimensionless equation (5), we can see that the characteristics of the change in the rising component of the T-S curve can be expressed by the curve in Equation (5).

$$T = T_r + (T_c - T_r)\{(d_m - S)/d_m\}^n \tag{2}$$

$$T = T_r + (T_c - T_r)(v_c\, t/d_m)^n \tag{3}$$

https://doi.org/10.52202/080513-0188

$$T - T_r = (T_c - T_r)(v_c t/d_m)^n \quad (4)$$

$$y = x^n \quad (5)$$

Figure 3 shows the curves for different values of the exponent/n in Equation (5). As the heating time/t progresses and the distance/S approaches zero, value of x in Equation (5) approaches 1.0 and value of y also approaches 1.0. For d_m being large, increasing the exponent/n can express a gradual increase in temperature, and for d_m being small, value of n can be made to approach zero to express a rapid increase in temperature. Temperature of the beam surfaces, or the charring temperature at the start of heating, can also be expressed by setting value of n to zero at t=0, i.e. when d_m being zero. All that remains is to find a function f_n (d_m) for continuously changing exponent/n, depending on the value of d_m.

As the surface of beam is assumed to reach the charring temperature at the same time as the heating start, f_n (d_m) must satisfy the condition of d_m = 0.0 and n = 0.0. In the n-d_m coordinates of Figure 4, where the vertical axis is the exponent/n and the horizontal axis is dm, f_n (d_m) must pass through the origin. The curve of f_n (d_m) calculated based on the data of the T-S curve of the specimen/PRF-b[3)] in the combustion test by Harada et al. shown in Figure 6 (to be described later) is shown in the Figure as a black solid curve.

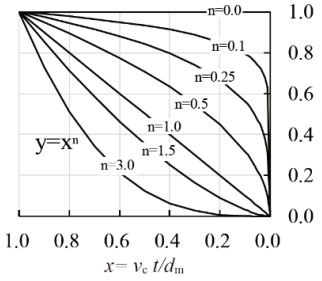

Figure 3: Curves by Eq.(5)

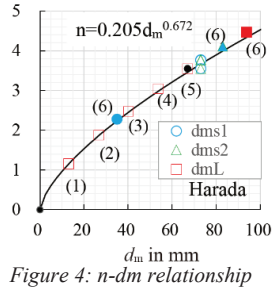

Figure 4: n-dm relationship of specimen 'PRF-b'

f_n (d_m) can be approximated by the exponential function Equation (7) passing through the origin. Symbols/○,△,□ in Figure 4 are plotted with values of n for d_{ms1}, d_{ms2}, and d_{mL}, used to approximate the mapped T-S curves for each of the coloured dotted curves in Fig. 6(b) for each measuring point in Fig.6(c).

$$n = A\, d_m^{\,B} \quad (7)$$

The constants A and B are specific values for each specimen, which are determined from the T-t curves measured for each specimen in individual combustion tests.

2.5 EXTRACTION OF T-S CURVE FROM TREE-DIERCTION HEATING

The temperature within wood of a beam under three-sided heating is expressed by Equation (8) based on the Assumption 2) and 5).

$$T = T_r + (T_c - T_r) \{ (v_c t / d_{mL})^{A\, d_{mL}^{B}} + (v_c t / d_{ms1})^{A\, d_{ms1}^{B}} + (v_c t / d_{ms2})^{A\, d_{ms2}^{B}} \} \quad (8)$$

As shown in Figure 1, there is a special point/m_{eq}, where d_{ms1}, d_{ms2} and d_{mL} are equal, and the temperature at the point/m_{eq} is expressed by Equation(9) from Equation(8).

$$T = T_r + (T_c - T_r)\, 3\, (v_c t / d_{meq})^{n_{eq}} \quad (9)$$

The value of the exponent n_{eq} can be determined by matching the T-S curve, which is mapped from the T-t curve obtained from the heating test to the curve that can be drawn by adjusting only the exponent n_{eq} in equation (9). For other points, the values of the constants A and B are found by arbitrarily giving them values in equation (8) and making the curve produced by equation (8) match the T-S curve for the target measurement point m, and the calculation load becomes large. In Figure 4, the curve in Equation (7) passes through the point (d_{meq}, n_{eq}) of point m_{eq}, so if

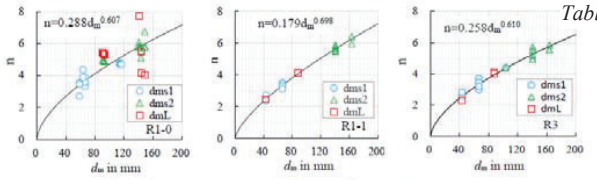

Figure 5: n-dm relationship by burning test's data

Table 1: Specimen's properties and coefficients for temperature

Specimen	Tree species	MC (%)	SG (kg/cm³)	CR (mm/min.)	A	B	α	Temperature of vaporization
Harada's PRF-b	A.S	-	-	0.617	0.205	0.672	0.5	110-150°C
R1-0	C.J.	12.2	0.39	0.615	0.288	0.607	0.5	110-150°C
R1-1	C.J.	9.9	0.37	0.615	0.179	0.698	0.5	110-150°C
R1-2	C.J.	10.4	0.36	0.615	0.189	0.686	0.5	110-150°C
R3	C.J.	10.2	0.35	0.615	0.258	0.610	0.5	110-150°C

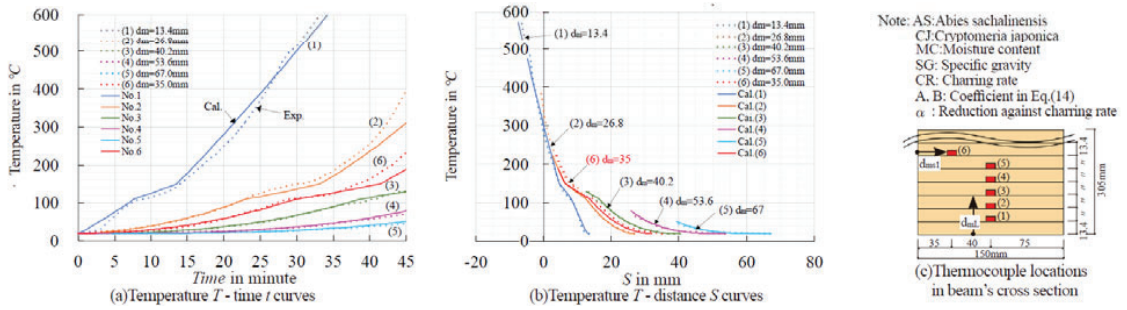

Figure 6: Temperature - time relationship of specimen 'PRF-b' of Harada's burning test for Abies sachalinensis

https://doi.org/10.52202/080513-0188

we substitute the coordinate values for the index n and d_m in Equation (7) and express both sides of the equation in logarithms, we get Equation (10), and the constant B is expressed in Equation (11).

$$\log_e n_{eq}=\log_e(A\, d_{meq}^{B}) \quad (10)$$

$$B=\log_e(n_{eq}/A)/\log_e(d_{meq}) \quad (11)$$

If you give a value of A, B can be calculated using Equation (11); the temperature/T can also be calculated using Equation (8), allowing you to draw a T-S curve. You can match the curve you draw, adjusting the value of A, to the T-S curve from the experiment. When making the match, values of n corresponding to d_{ms1}, d_{ms2}, and d_{mL} for each measurement point are calculated using Equation (7).

The values of n corresponding to d_{ms1}, d_{ms2}, and d_{mL} for the matched stage are shown in the symbols in Figure 4. The results of calculation for the specimen/PRF-b[4] of Harada et al. are shown in Figure 6(b). The T-S curves (dotted curves) for each point in Figure 6(c) are illustrated using dm as the minimum value of d_{ms1}, d_{ms2}, and d_{mL}. Values of A and B for each measuring point were adjusted so that the curve (solid curve) based on Equation (8) matches the curve (dotted curve).

As the charring rate/v_c is assumed to be the same constant value regardless of the heating direction, it is also possible to specify A and B for the T-S curve where dm is either d_{ms1}, d_{ms2}, or d_{mL}. However, points (1) to (5) in Figure 6(c) have the same value of 75 mm for d_{ms1} and d_{ms2}, and if we assume that the value is dm, then the start of heating at each measuring point in Figure 6(b) will overlap at the 75 mm position on the S axis, and the relationship between the shortest charring distance and temperature rise will become unclear. The curve for the relationship is not suitable for identifying the values of A and B. It is sufficient to select a suitable d_m for determining the values of A and B at each measuring point. Values of A and B for each component from 3-direction are determined by finding the curve that matches the T-S curve in Figure 6(b) in the range of 20-110°C before the effect of the evaporation of wood's moisture owing to heating, using Equation (8). In this case, we selected the point (5) for point m_{eq} and carried out the calculation. The data for the point (5) is shown as a black circle in Figure 4. Although the point (5) does not satisfy the condition for point m_{eq} in Figure 1, it is the closest point. The closer the point selected is to the point/m_{eq}, the dramatically less work is required to determine the values of A and B that match the T-S curve. In Figure 6(b), the dotted curves are the T-S curve mapped from the T-t curve of the experiment. The distribution of the values of n used to calculate the curve at each position is shown by symbols/○,△,□ in Figure 4. The point (6) has the smallest d_{ms1}. The other points have the smallest d_{mL}. In the Figure, the data are almost on the black solid curve. The solid curves in Figure 6 (a) and (b) were calculated using the approximation formula for n in Figure 4. In Figure 6 (b), the solid curve calculated accurately estimates the dotted experimental T-S curve in the range below 110°C. It is demonstrated that the T-S curve of one-direction heating can be extracted from the T-t curve measured under three-direction heating.

2.6 RATE OF TEMPERATURE RISING UP TO CHARRING TEMPERATURE

At temperatures above 110°C, the evaporation of wood's moisture becomes more pronounced; hence, the rate of temperature rise slows down. The charring rate/v_c, which is, as a result, mapped onto the T-S curve using Equation (1), is determined based on the charring temperature, so the rate is necessary to be linked to the rate of temperature rise in the T-t curve. The phenomenon is still also shown in Figure 2. In the range of the evaporation, it is necessary to slow down the charring rate. Let the rate of deceleration be α, and the velocity in the range be $\alpha\, v_c$. However, because the time it takes to reach the charring temperature is delayed, it is necessary to accelerate the charring rate after the upper limit temperature of the vaporisation. The rate/β of acceleration of the charring velocity is expressed by Equation (12). Let the lower limit temperature at which moisture evaporates be 110°C, and the upper limit temperature of the range be 150°C.

$$\beta=\{ v_c t_c - v_c t_{VaL} - \alpha\, v_c(t_{VaU} - t_{VaL}) \}/(t_c - t_{VaU}) /v_c \quad (12)$$

$$\beta=\{ t_c - t_{VaL} - \alpha (t_{VaU} - t_{VaL}) \}/(t_c - t_{VaU}) \quad (13)$$

where, $t_c=d_m/v_c$, t_{VaL}, t_{VaU}: the time it takes to reach the lower and upper limits of vaporization temperature

2.7 FOUNCTION FOR ESTIMATING TEMPERATURE PROFILE IN THE BEAM SUBJECTED 3-DIRECTION HEATING

By rearranging the above, the formula for estimating the temperature is expressed as Equation (14).

$$T= T_r + (T_c - T_r)\{(x /d_{mL})^{A d_{mL}^{B}} + (x/d_{ms1})^{A d_{ms1}^{B}} + (x/d_{ms2})^{A d_{ms2}^{B}} \} \quad (14)$$

where $0°C<T\leq 110°C$: $x = v_c\, t$, $110°C<T\leq 150°C$: $x = x_{110}+\alpha\, v_c\, (t-t_{110})$, $150°C<T$: $x = x_{150}+\beta\cdot vc\cdot(t-t_{150})$, where x_{110}, t_{110}: values of distance x and heating time t when 110°C is reached, x_{150}, t_{150}: values of distance x and heating time t when 150°C.

The basic form of this function is the same as formula by W. Klingsch et al. [4], and A. Frangi et al. [5] have limited it to 20-200°C and modified the exponential component. The differences between these formulas and our method are the range of temperature and that the exponential part is dependent on the depth/d_m of the wood at each point, not the carbonisation time t, and that the evaporation of the moisture in wood is considered.

2.8 TEMPERATURE-TIME CUREVE CALCULATED

https://doi.org/10.52202/080513-0188

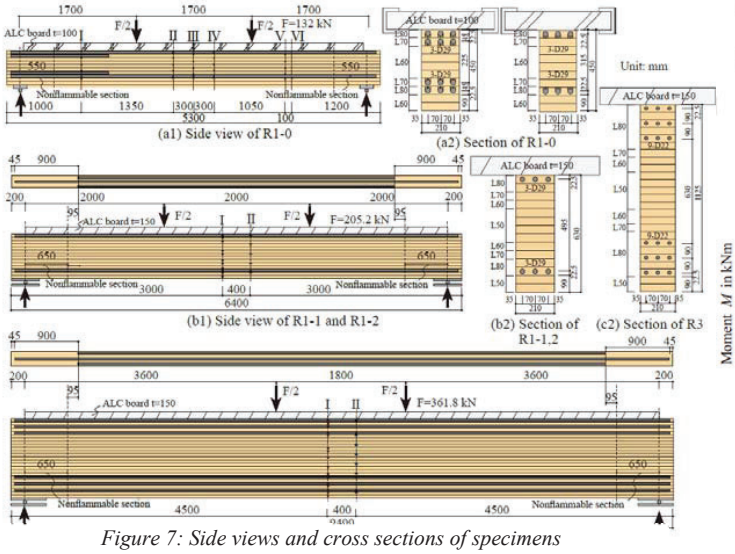

Figure 7: Side views and cross sections of specimens

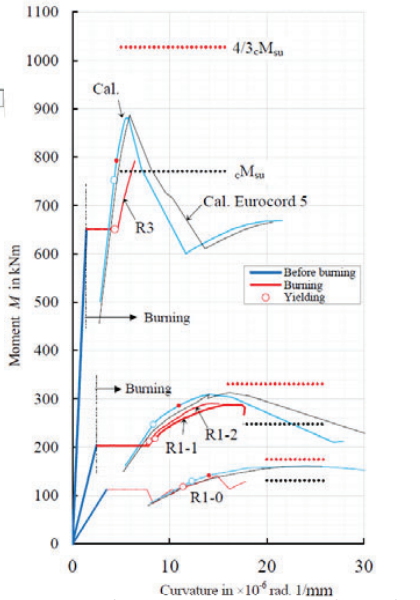

Figure 8: Bending moment-curvature relationship

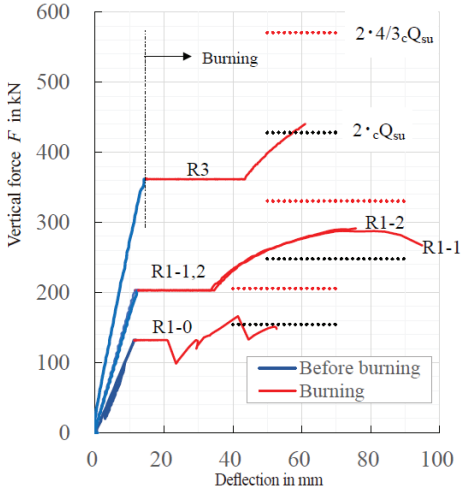

Figure 9: Force-deflection relationship

The suitability of the *T-t* curve obtained using the above estimation method was also verified for our specimens and all specimens from other researcher specimens in Japan. Due to space limitation of this paper, the suitability of these test pieces cannot be shown here.

Table 1 shows a list of the specimens, species, moisture content, oven-dry specific gravity, charring rate, constants A and B, deceleration ratio α and temperature of moisture vaporisation. The charring rate was assumed to be the average of the charring rates at several measurement points where their temperature reached 300°C for each test specimen. The depth of wood of d_{mL}, d_{ms1}, d_{ms2} was the shortest distance to the groove of a thermocouple. The dimension of the groove was assumed to be 3x2mm.

As can be seen in Figure 6(b), the solid line of the calculation for the specimen of Harada et al. almost estimates, with high degree of accuracy, the dotted *T-S* curve of all measurement points. This means that we were able to specify appropriate the charring rates/v_c and βv_c and the constants *A* and *B*.

The same is shown for our specimens in Figure 7-18. Please, details of the Figures are referred to Reference 2 and 3 published in WCTE 2023 and WCTE 2025. The numberings of the points marked as m_{eq} are shown in red characters in Figure 12(g) and Figure 16. Figure 12(a) shows change in temperature at all measuring points of R3. Figure 12(b) shows change in temperature at the boundary of the central element and the points inside it. Points of 6 to 40 are at the boundary, and the depth of wood on the side is the same, so the calculated values are almost the same and are not affected by d_{mL}. However, the experimental values of the temperature varied regardless of the vertical locations. This variation includes the influence of the steel bars, but the influence was not clear in the locations. Their variation was ±15°C compared to the median value at 42-72°C during the 60-minute heating period. As a main purpose of modelling the temperature distribution is to estimate the strength capacity of beam, it is important to estimate the average of the experimental temperatures at the same d_m.

The numbering in the Figures, such as Cal.1, indicates the numbering of the measuring point calculated. The thin curves for Cal.4-60 roughly estimate the median of the experimental curves at the points/ 4 to 60. The temperature rise at the central points of the beam width is small, but the thin curves of the calculated values also estimate the changes. Figure 10(c) shows the change in temperature at representative points with different d_m. The thin curves of the calculated values roughly estimate the dotted curves of the experiments even when d_m differs.

Figure 12(d) shows change in temperature of rebars. The effect of the rebar's thermal capacity is ignored and the temperature of wood at the position is assumed to be equal to the temperature of rebar. Temperature of the side rebar, where the depth of wood to the rebar's groove is approximately 22mm, increases at a faster rate from 10 minutes onwards. The curve calculated for the location of the thermocouple in Figure 13 is shown as Cal.A, and the curve calculated for the center of rebar is shown as Cal.B.

https://doi.org/10.52202/080513-0188

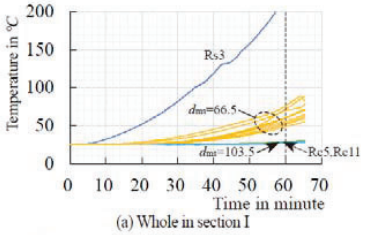

(a) Whole in section I

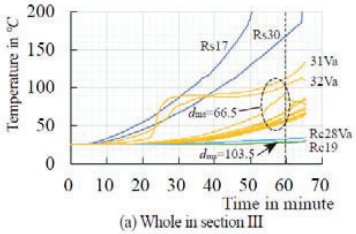

(a) Whole in section III

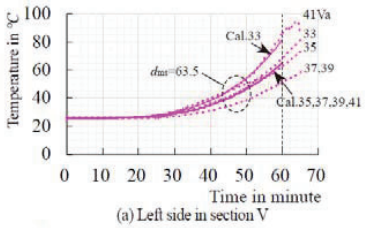

(a) Left side in section V

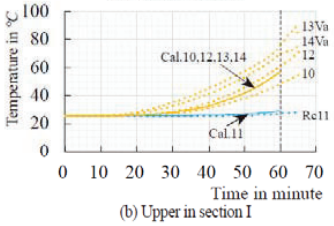

(b) Upper in section I

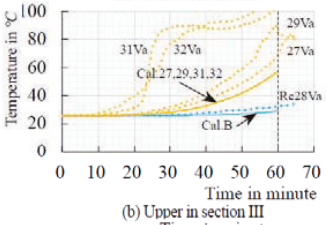

(b) Upper in section III

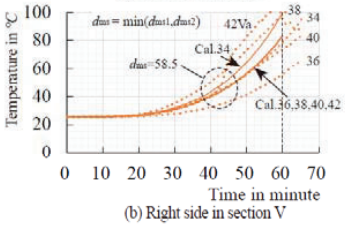

(b) Right side in section V

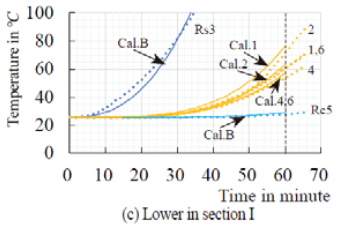

(c) Lower in section I

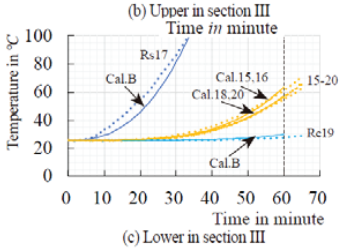

(c) Lower in section III

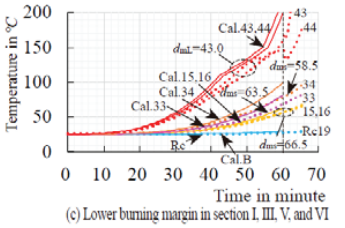

(c) Lower burning margin in section I, III, V, and VI

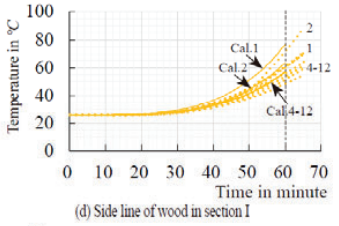

(d) Side line of wood in section I

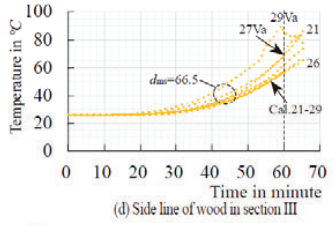

(d) Side line of wood in section III

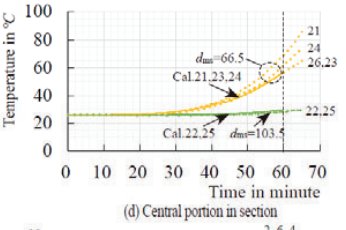

(d) Central portion in section

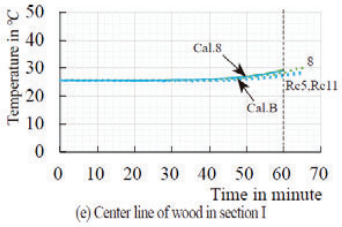

(e) Center line of wood in section I

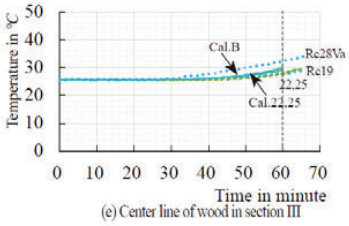

(e) Center line of wood in section III

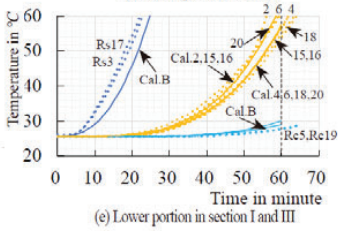

(e) Lower portion in section I and III

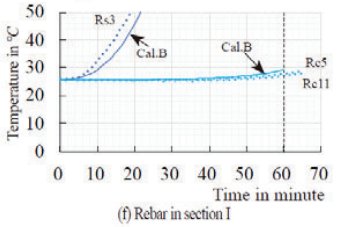

(f) Rebar in section I

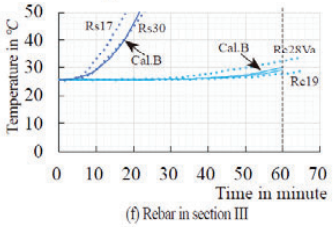

(f) Rebar in section III

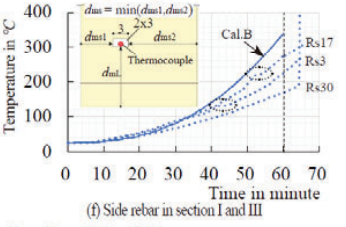

(f) Side rebar in section I and III

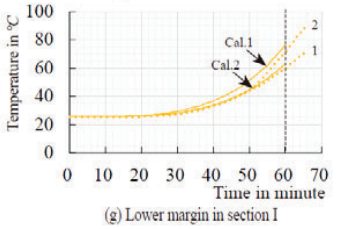

(g) Lower margin in section I

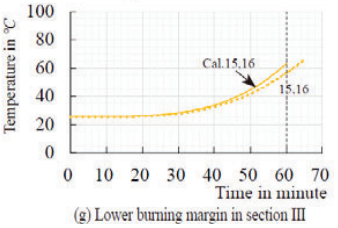

(g) Lower burning margin in section III

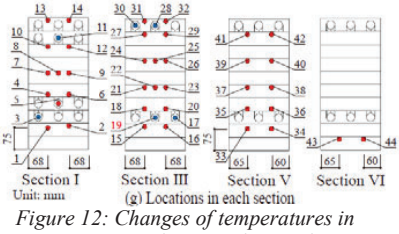

(g) Locations in each section

Figure 10: Changes of temperatures in section I of R1-0

Figure 11: Changes of temperatures in section Ⅲ of R1-0I of R1-0

Figure 12: Changes of temperatures in section V, lower and central portions, and side rebars of R1-0 etc.

https://doi.org/10.52202/080513-0188

Temperatures of the side rebar generally vary between the two curves. However, since the side rebars exist in the charred zone and does not resist after heated for 60 minutes, the accuracy of the estimation of their temperature is not a problem from the perspective of estimating the strength capacity of beam. For the central rebars, values of Cal.A and Cal.B are nearly equal, and their calculations is almost estimated the experimental curves. The degree of conformity between these experimental and calculated values was generally the same for R1. In points 10 and 15 of Figure 14(c), the calculated temperature rise slows down after 45 minutes. This is due to the excessively small value of α, the rate of deceleration of charring in the range where moisture evaporates. Local variations need to be considered when estimating temperature. The curves calculated are also shown in Figures 10-12.

Excluding the point V_a, which is said to be affected by moisture vapour on the top surface of beam in Figure 11(b), the curves calculated estimate the experimental curves with the same level of accuracy as the specimens in Figure 13-15. The gap between the slab and the beam top surface due to deflection probably caused the temperature to rise more quickly. The location of the thermocouple around side rebar in the specimen was unknown, so only Cal. B, which is the centre of the rebar, is shown in Figure 10(c) and Figure 11(c).

3 – VERIFICATION OF TEMPERATURE PROFOILE, STRESS PROFILE, AND

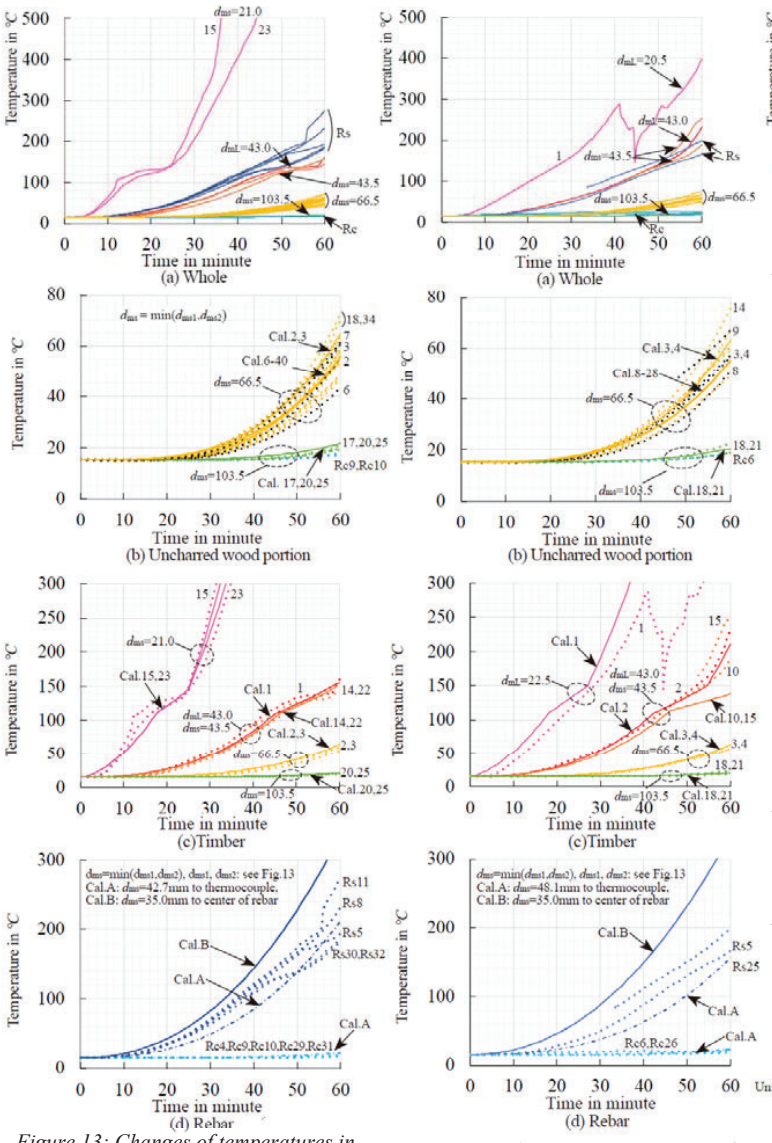

Figure 13: Changes of temperatures in section I of R1-0

Figure 14: Changes in temperature of R1-1

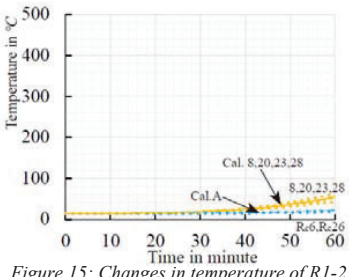

Figure 15: Changes in temperature of R1-2

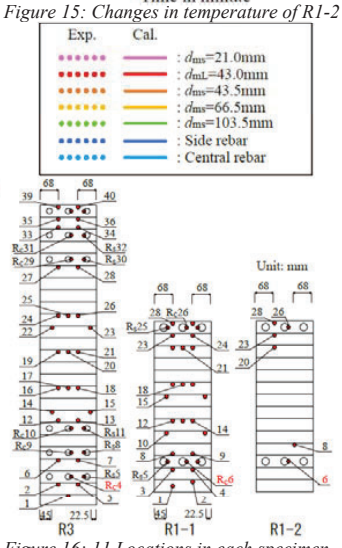

Figure 16: 11 Locations in each specimen

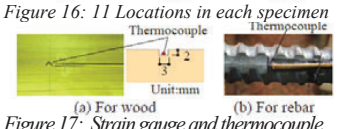

Figure 17: Strain gauge and thermocouple

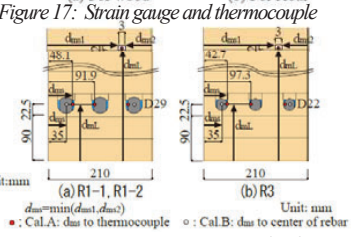

Figure 18: Locations around rebar

https://doi.org/10.52202/080513-0188

STRENGTH OF WOOD DURING HEATING

3.1 PROFILES OF TEMPERATURE AND REDUCTION OF ELASTIC MODULUS AND STRENGTH OF WOOD

3.1.1 Temperature profile

The cross-section was divided into 84 elements in the beam width direction, 180 elements in the beam height direction for R1-0, 252 elements for R1-1,2, and 450 elements for R3, and the dimension of each element was set to 2.5x2.5mm. If the values of d_{mL}, d_{m1} and d_{m2} at the centre of the area element are given, the temperature can be calculated using Equation (14). The constants/A and B employed values in Table 1. The effect of rebar thermal capacity was ignored. Figure 20 on the next page shows the temperature profile in the cross-section of the beam when heated for 60 minutes. Figure 19(a) shows the profile of isotherms in the right half of the cross-section of R1-0 shown in Figure 19(b). The view is from the top to the bottom of the beam section; charred zone is assumed to be at above 300°C.

The temperature drops sharply, as entering from the charred border into the uncharred zone. The x-y coordinate axe is shown as Figure 19(b). The origin of x and y is the point at the center of the beam width at the boundary between the structural section and cladding lamina. The y-axis is positive in the upward direction, and negative means the range of cladding lamina mentioned in Reference 2 and 3.

The curves for the temperature in the beam height direction are shown on the left of Figure 19(c)(d). x=0mm is the center of the beam width, x=±35mm is the boundary of the central element, and x=±70mm is the centre of the end rebar.

3.1.2 Reduction in elastic modulus and strength due to temperature rise

Figure 20 shows reduction factor curves in in elastic modulus and strength. In Eurocode 5[6], the reduction in design is set at a conservative level based on existing collected data. In Japan, there is the research of Kaku and Hasemi et al.[7]. They conducted bending test on square timber (cross-section: 20 x 20 mm) to investigate

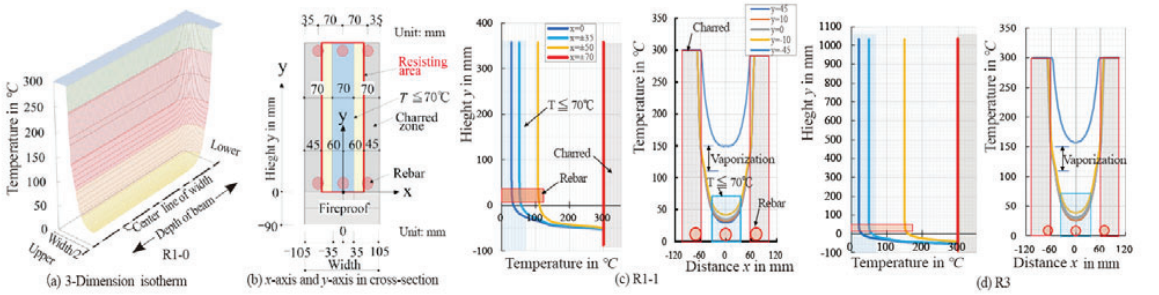

Figure 19: Temperature profile of wood in beam's section calculated by the new concept after 60-minute burning

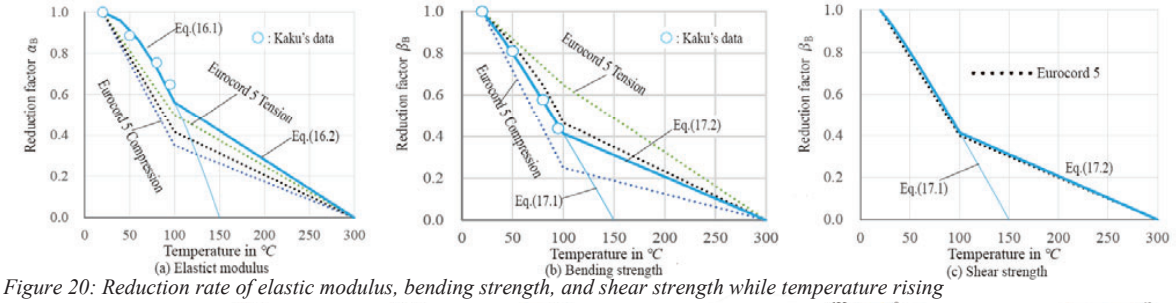

Figure 20: Reduction rate of elastic modulus, bending strength, and shear strength while temperature rising

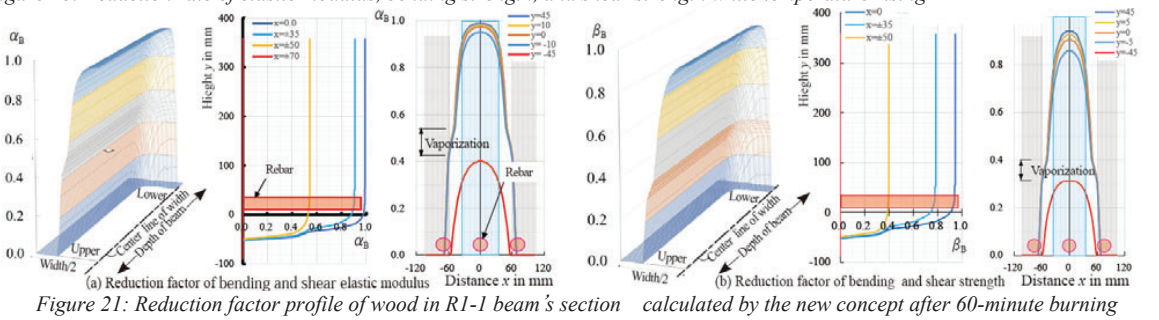

Figure 21: Reduction factor profile of wood in R1-1 beam's section calculated by the new concept after 60-minute burning

https://doi.org/10.52202/080513-0188

the effects of temperature and moisture content systematically, limiting the species and moisture content, and reported the reduction rates of the bending Young's modulus and bending strength. Out of these data, the distribution of the reduction rates (average values) for each species and moisture content that match the test conditions, i.e. Japanese cedar with a moisture content of 5-15%, is shown in Figure 21 using a circle symbol. The reduction rate is the ratio of the value at each temperature to the experimental value at 20°C. The approximate equations for the circle symbols are shown in Equations (16.1) and (17.1). The curves for each equation are shown in Figure 20 as thin blue curve.

For Young's modulus

$0 \leqq T \leqq 100$℃: $\alpha_B = 1 - \{(T-20)/130\}^{1.7}$ (16.1)

100℃<T: $\alpha_B = \alpha_{B100}/200\,(300-T)$ and $\alpha_B \geqq 0.0$ (16.2)

where, α_{B100} : the value obtained by subsuming 100℃ for T of Equation (16.1)

For bending strength

$20 \leqq T \leqq 100$℃: $\beta_B = 1 - \{(T-20)/130\}^{1.1}$ (17.1)

100℃<T: $\beta_B = \beta_{B100}/200(300-T)$ and $\beta_B \geqq 0.0$ (17.2)

where, β_{B100} : the value obtained by substituting 100℃ for T of Equation (17.1)

The reduction factor for tension (green) and compression (blue) of Eurocord 5 are shown in the same Figure as dotted curve. The reduction factors of Young's modulus and flexural strength calculated by applying these to the compressive and tensile regions of a rectangular-section material subjected to bending are shown by the black dotted curve. These reduction factor curves are intermediate between the compressive and tensile reduction curves. The reduction factor of flexural Young's modulus of Kaku [6] et al. is higher than that of Eurocord 5 up to 100℃, and flexural strength curve is close to that of Eurocord 5 up to 100℃. Herein, the reduction rate is assumed to be the value obtained from Equations (16.1) and (17.1) up to 100℃, and from 100℃ to 300℃, the values obtained from the straight line connecting the point at 100℃ and the point of the factor=0.0 at 300℃ each. These are indicated by the bold blue curve.

The distribution of the reduction factor in the flexural modulus and flexural strength calculated in accordance with the temperature profile in Figure 19 is shown in Figure 21, respectively. Factor of the range in which the moisture content of the wood evaporates decreases gradually in the direction of the beam width.

3.2 ESTIMATION OF STRESS PROFILE AND STRENGTH CAPACITY

Figure 22 shows the shape of stress-strain relationship for wood when using the reduction rates of Kaku et al. and Eurocord 5. Figure 23 shows the stress-strain relationship for wood under bending, which uses the Young's modulus and strength of wood, and the stress-strain relationship for rebar. Figure 24 shows a schematic diagram of the cross-section to be resisted and the strain distribution. The depth of carbonisation due to the bending of the side rebar during heating was also taken into account, and the outer 10mm range around the end rebar (the square range enclosed by the thick black line) was also assumed not to resist. Other than these, the reduction rate of the elastic modulus and strength due to the rise in temperature was taken into account. The central reinforcement was assumed to resist without being affected by temperature. Assuming that the cross-section maintains its plane section after bending, the strain/ε_{wc} of the compression edge of the top surface, , was increased in fixed increments, and the strain/ε_{wt} of the tension edge, was adjusted so that the resultant force in the cross-section converged to zero at each stage. Moment and curvature were calculated by performing incremental analysis of general bending. Figure 26 shows the contours of bending stress in wood with in the beam cross-section for the calculated maximum load, which is the same as the experimental

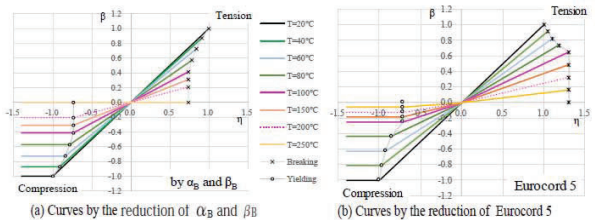

Figure 22: Stress - strain curves obtained by α, β and Eurocord5

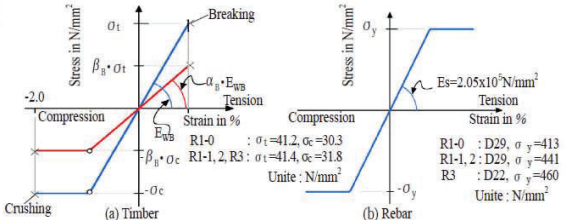

Figure 23: Stress - strain curves assumed for calculation

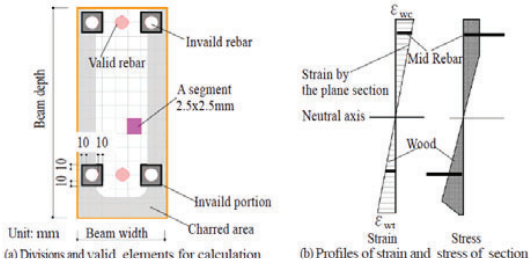

Figure 24: Valid segment, rebars, and strain profile for bending capacity

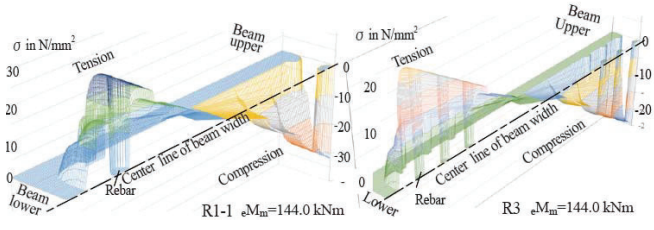

Figure 25: 3-Dimension isotherm of normal stress of wood of beam's section

https://doi.org/10.52202/080513-0188

maximum load; the left half of the beam width in Figure 20(b) is shown as a view from the bottom surface of the beam to the top surface. Rebar portions are illustrated as zero stress. The bottom side is the flexural tension zone and the top side of the beam is the flexural compression zone. Figure 27 shows an example of a contour curve of the magnitude of the calculated shear stress in wood in the beam cross-section when the beam is subjected to the same shear force as in the experiment at maximum load. Moment-curvature relationship (M-ϕ relationship) calculated is shown in Figure 8 as a light blue curve. The ○ (experiment) and ○ (calculation) points are the points at which tensile rebars yielded in tension. The ● point is one at the maximum load point in the experiment. The range before and after the maximum moment is shown. Also, Figure 8 shows M-ϕ relationship calculated using stress-strain curve of Eurocord 5 in Figure 22(b), shown as black curve. Its stiffness is lower than the light blue curve, and it approaches the experimental relationship, but the flexural capacity is almost the same as the capacity of the light blue curve.
On the basis of the assumption of plane section after bending, shear stress in the shear span of the beam can be calculated. The shear stress can be calculated from the ratio of the shear modulus Gi at the center segment divided, as shown in Figure 26(b), to the resultant force F in the axial direction of the beam material at any height in the horizontal plane of the small section dx in the axial direction of the beam material, as shown in Figure 26(a). Figure 27 shows an example of the shear stress profile calculated at the maximum load for R3. The shear ultimate strength capacity/$_cQ_{su}$ of the beam was assumed to be the shear force of the beam when the maximum value of the shear stress was equal to the shear strength of the wood F_s (2.7 N/mm^2). As the shear strength of wood also varies, the upper limit of its strength was set at 4/3 times the value/F_s. Figure 9 shows the load that balances it, indicated by red and blue horizontal dotted lines. Figure 8 also shows the moment that balances those in the same way. The details cannot be described here due to space limitations, but these calculation results were able to explain the experimental results. For details, please refer to the literature [8].

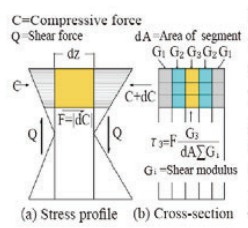

Figure 26: Calculation of shear stress

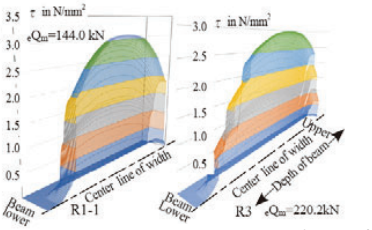

Figure 27: 3-Dimension isotherm of shear stress on beam's section

4 – SUMMARY

To estimate strength capacities of steel bar-timber composite beam heated for 60 minutes of heating, a method was proposed to estimate the temperature profile in the uncharred portion inside the beam from the measured temperature-heating time curve in a combustion test, and calculation for the beam under bending was carried out using reduction rates of Young's modulus and strength to reveal the stress distribution in the wood cross-section and strength capacities of beam. The results are summarized below.

i) We proposed equations for estimating the temperature of uncharred portion, which maps a temperature-heating time curve inside a beam onto a temperature-charred border distance curve (T-S curve), and approach for determining the constants in the equation by fitting the T-S curve to the temperature-charred border distance curve of a beam tested. As wood is a natural material, there will be variations in temperature even at the same location within a section under the same conditions, but temperatures calculated by the proposed method estimated approximately temperature-time curves of wood obtained within a beam from the combustion test of the beam.

ii) The temperature profile estimated using the proposed method, and the flexural strength, shear strength and moment-curvature relationship calculated using the existing reduction factor of Young's modulus and strength with the temperature profile, were able to explain the results of the experiment in general.

5– REFERENCES

[1] S. Shioya, et al.: An innovative hybrid timber structure in Japan: performance of column and beam, Wein, WCTE 2016

[2] S. Matsushita and S. Shioya: Burning test of steel bar - timber composite beam, Oslo, WCTE 2023.

[3] S. Shioya and S. Matsushita, S. Shioya: 60-minute combustion test under loading of steel bar-timber composite beams, Brisben, WCTE 2025

[4] W. Klingsch et al.: Temperaturentwicklung in brandbeanspruchten Holzquerschnitten, Fraunhofer IRB Verlag,1993.

[5] Andrea Frangi, et.al: Charring rates and temperature profiles of wood sections,FIRE AND MATERIALS, Fire Mater. 2003; 91–102

[6] C. KAKU, et at.: Influence of moisture content of wood on the structural properties under high temperature, Vienna, WCTE 2016

[7] Eurocode 5, Design of timber structures - Part 1-2 General -Structural fire design, EN 1995-1-2, EUROPEAN COMMITTEE FOR STANDARD-IZATION, 2004

[8] S. Shioya and S. Matsushita: Estimation of temperature profile, and strength of steel bar-timber composite beam on 60-minute fire resistance test, Journal of Structural and Construction Engineering (Transactions of AIJ), Vol. 90, No. 828, 218-229, Feb., 202 (in Japanese)

https://doi.org/10.52202/080513-0188